

We are IntechOpen, the world's leading publisher of Open Access books Built by scientists, for scientists

6,900

Open access books available

186,000

International authors and editors

200M

Downloads

Our authors are among the

154

Countries delivered to

TOP 1%

most cited scientists

12.2%

Contributors from top 500 universities



WEB OF SCIENCE™

Selection of our books indexed in the Book Citation Index
in Web of Science™ Core Collection (BKCI)

Interested in publishing with us?
Contact book.department@intechopen.com

Numbers displayed above are based on latest data collected.
For more information visit www.intechopen.com



Synthesis of Metal Oxide Semiconductor Nanostructures for Gas Sensors

Nazar Abbas Shah, Majeed Gul, Murrawat Abbas and Muhammad Amin

Abstract

Zinc oxide (ZnO) is a unique and important metal oxide semiconductor for its valuable and huge applications with wide band gap (3.37 eV) and most promising candidate for gas sensor due to its high surface-to-volume ratio, good biocompatibility, stability, and high electron mobility. Due these properties, metal oxide shows good crystallinity, higher carrier mobility, and good chemical and thermal stability at moderately high temperatures. In this chapter nanostructures have been investigated, main focus being their synthesis and sensing mechanism of different toxic chemicals, synthesized by thermal evaporation through vapor transport method using vapor-liquid-solid (VLS) mechanism. The doped ZnO nanobelts showed significant enhanced sensing properties at room temperature, indicating that doping is very much effective in improving the methane CH₄ sensing of ZnO nanostructures. ZnO nanowires showed a remarkable sensing response toward acetone and CH₄ gas.

Keywords: metal oxide, semiconductor material, Mg doping, nanobelts, structural and morphological properties, band gap, gas sensing

1. Introduction

From the last decade, nanotechnology has established a bridge among all the fields of science and technology. Low-dimensional materials and structures have exceptional properties that make them able to play a critical role in the rapid progress of field science. With these excellent properties, 1-D metal oxide semiconductors (MOS) have become the backbone of research in all fields of natural sciences.

Nanotechnology deals with structures and materials of very small dimensions. Nanotechnology is the foundation and exploitation of nanomaterial with structural features in between those of atoms and their bulk material. The properties of the materials at nanoscale are extensively different from those of bulk materials. The high surface reactivity with the surrounding surface improves significantly. When the size of materials is in the nanoscale, the surface-area-to-volume-ratio (L/D) becomes large that makes the nanomaterial ideally an appropriate candidate for many types of sensing applications. That is why nanomaterial has opened up possibilities for new pioneering functional devices and technologies. Nanostructures have at least one dimension less than 100 nm. Crystal structures are much stable at nanoscale [1].

Reduction of an object size results in large surface to volume ratio hence the surface turn out to more vital and that large surface to volume ratio greatly affected the chemical, electrical and optical properties of nanomaterials. Quantum effects owing to size confinement in nanostructures occurs, when the typical size of the object is equivalent to the crucial length (range 1–10 nm) of the equivalent physical properties' screening length, then the mean free path of electrons; 0-D quantum dots, 1-D quantum dots, and 2-D quantum well are the characteristic structure forms.

Low power consumptions, best crystallinity, and high integration density 1-D with high aspect ratio are shown by the 1-D nanostructures. The nanostructure materials show high sensitivity to surface chemical reactions, with increased surface-to-volume ratio and a Debye length matching with small size. Tunable band gap is enabled by size confinement [2]. In the recent past, various synthesis methods, such as vapor phase method, electrochemical method, liquid phase methods, and solution-gel methods, were used. Out of these growth techniques, vapor transport method, using vapor-liquid-solid (VLS) growth mechanism or VS growth, is one of the finest growth techniques used for the growth of metal oxide semiconductor nanostructures. It is a cost-effective easy method used to create many single-crystalline 1-D nanostructures [3–11].

Smart and functional materials are based on metal oxides [10]. Synthesis and fabrication of devices based on metal oxide semiconductor have become more important recently, because the tuning of physical properties of these metal oxides is so easy. Among these MOS, ZnO is a material that has strong piezoelectric and optical properties on the bases of its wide band gap, stability at high temperature, large surface-to-volume ratio, and high excitonic binding energy. They are used in solar cells, photocatalysis, and antibacterial active material. Therefore research work has been carried out on ZnO nanostructures. Metal oxide materials possess electrical, chemical, and physical properties that are highly sensitive to the changes in a chemical environment, through a variety of detection principles based on ionic, conducting, photoconducting, piezoelectronic, pyroelectronic, and luminescence properties [12–21].

Doping is another technique utilized to improve ultraviolet (UV) sensing properties of metal oxides, where the dopant atoms are believed to act as activators for surface reactions. In MOS, the electrical, optical, and chemical properties can be changed by adding the doping materials or by creating oxygen defects which results in large concentration of carriers, mobility, and electrical resistivity. So doping offers another avenue for expanding their sensing capability [12].

Up to now, various metal oxides' 1-D nanostructures (SnO_2 nanowhiskers, In_2O_3 nanowires, ZnO nanorods, WO_3 nanowires, TiO_2 nanowires etc.) have been fabricated into film-type nanosensors by means of thermal evaporation or vapor transport method. The most widely studied substances are SnO_2 and ZnO nanowires [13]. In this research work, 1-D n-ZnO nanostructures (nanowires, nanorods, nanobelts with needle-like ends, and typical nanobelts) were grown by using vapor transport method using VLS mechanism on n-type Au-coated silicon substrate Si (100). The electrical and optical properties of ZnO nanostructures were investigated using different characterization techniques [14–37].

2. Important properties of metal oxide semiconductors

As work done in this chapter mainly deals with ZnO semiconductor, structural properties of ZnO material are presented below.

2.1 Structural properties of ZnO

ZnO is a key technological and prominent material. One of the important properties of ZnO is that it has a wide band gap that makes it suitable for optoelectronic applications of short wavelength. ZnO has high excitonic binding energy (60 meV) at room temperature by ensuring efficient excitonic emission. It has been noted that disordered nanoparticles and thin films at room temperature have ultraviolet (UV) luminescence. In addition, due to the unavailability of centrosymmetry in wurtzite structures that combines with large electromechanical coupling which result in strong piezoelectric and pyroelectric properties and make ZnO a prominent material in the use of mechanical actuators and piezoelectric sensors. As a versatile functional material, ZnO has a different group of growth morphologies, such as nanocombs, nanowires, nanobelts, nanosprings, etc. These ZnO nanostructures are easily obtained, even on cheap substrates such as glass. As work done in this thesis mainly deals with ZnO semiconductor, structural properties of this material are presented below.

2.2 Crystal and surface structure of ZnO

At normal temperature and pressure, ZnO crystallizes in wurtzite (B4 type) structure, as shown in **Figure 1**. It is a hexagonal lattice, belonging to the space group P63mc with lattice parameters $a = 0.3296$ nm and $c = 0.52065$ nm. The tetrahedral coordination in ZnO is responsible for noncentral symmetric structure and consequently results in piezoelectricity and pyroelectricity. Another important characteristic of ZnO is polar surfaces. The most common polar surface is the basal plane. The oppositely charged ions produced positively charged Zn^+ (0001) and negatively charged O^- ($000\bar{1}$) surfaces, which result in a normal dipole moment and spontaneous polarization along the c -axis as well as variance in surface energy. The two most commonly observed facets for ZnO are $(2\bar{1}\bar{1}0)$ and $(01\bar{1}0)$ which are nonpolar surfaces and have lower energy than the (0001) facets [14, 15]. ZnO has varied properties, covering all of its physical, chemical, or material properties.

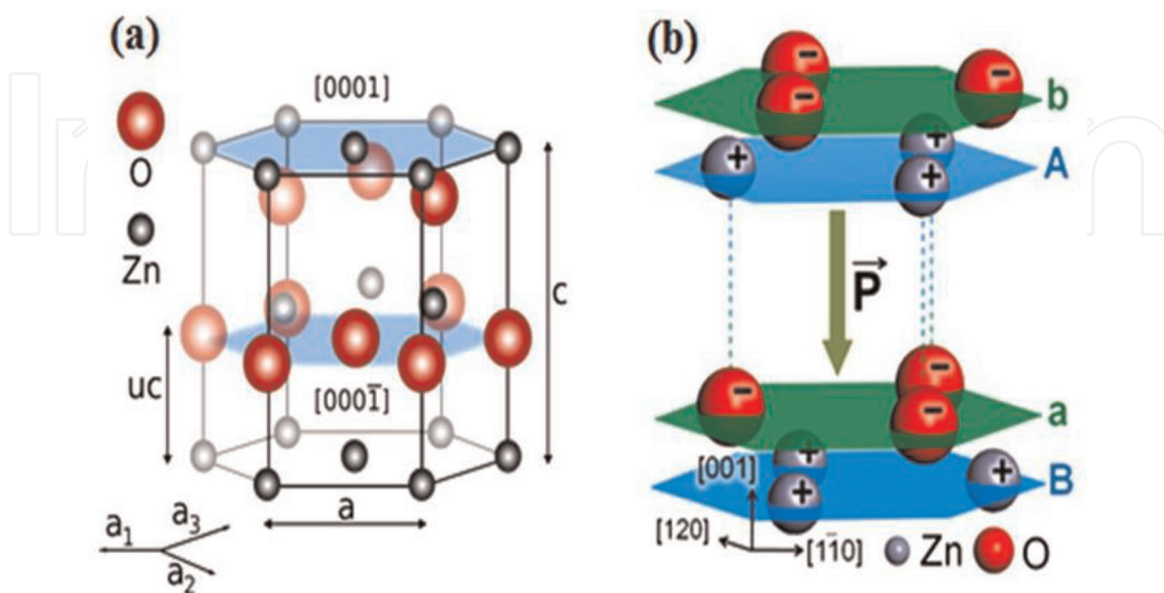


Figure 1.

(a) Crystal structure of hexagonal wurtzite ZnO, ZnO unit cell, including the tetrahedral coordination between Zn and its neighboring O. (b) ZnO has a noncentro-symmetric crystal structure that is made up of alternate layers of positive and negative ions, leading to spontaneous polarization.

ZnO is a well-suited II–VI wide bandgap semiconductor, which is naturally found in three forms: cubic zinc blend, hexagonal wurtzite, and cubic rock salt which is not as common as other [16]. The most common phase of ZnO is hexagonal wurtzite, whose space group is C6v or P63mc, which can be found mainly in ambient condition [17].

In **Figure 1(a)** is a crystal structure of ZnO which is a combination of alternating planes with tetrahedral coordination of Zn^{+2} and O^{-2} ions along the c-axis. Due to the presence of polar surfaces, ZnO crystal becomes spontaneously polarized in two type of planes, i.e., tetrahedrally coordinated O^{-2} and Zn^{+2} ions stacked alternately along the c-axis.

2.3 Gas sensing properties

In recent times due to environmental pollution and other chemical hazards, the needs for the development of a trusted chemical sensor have been significantly increased. For sensing of trace vapor of chemicals, different types of sensors, for example, potentiometric, fiber optics, amperometric, and biological sensors, are used, but ZnO nanostructure-based sensor has its own importance owing to its stability, high sensitivity, selectivity, as well as wide operating temperature range and flexibility in processing during device fabrication [18–24].

High surface area, well organized molecular structure, and single crystalline make ZnO nanostructures unique and prominent candidates for gas sensing application. Gas attachment sensing mechanism, such as O^{-} , O_2 , H^{+} , and OH^{-} contact as analytes that result in change in the electrical conductivity of the charges, is mainly dependent on the redox reaction. This process can only be activated by activation energy because the classic metal oxide semiconductor sensors only operate at a temperature higher than 200°C. Because of the significant changes in optoelectronic properties at nanoscale, the problem of power consumption might be tackled, and the sensor with low energy consumption can operate even at room temperature. On exposing the surface of sensor to air, attachment of O or O_2 takes place. Due to these attachments of O or O_2 on the nanostructure surface, formation of space charge region with high resistivity takes place. Due to high aspect ratio (L/T), the nanobelt nanostructure surface give rise to a high resistance in the normal state; this is due to the thin thickness of nanobelt nanostructures that offer a significant amount of surface acceptor states. The removal of chemisorbed oxygen from nanostructure surface by chemical reaction on the surface of nanostructures results in the improvement of conductance of nanostructures in chemical environment as shown in **Figure 2**.

2.4 Gas sensors based on metal oxide semiconductor nanostructures

It is important to note that two main types of semiconducting metal oxides exist which are used in chemiresistive sensors. The first one is n-type semiconductors (conductance increases, when redox reaction takes place on the surface of nanostructures, e.g., TiO_2 , ZnO, and SnO_2) whose majority carriers are electrons. The second type of metal oxides used is p-type semiconductors (conductance decreases, when redox reaction takes place on the surface of nanostructures, e.g., NiO and CuO) whose majority carriers are holes. The majority of semiconducting metal oxides used in chemiresistive sensors are n-type because electrons are spontaneously produced via oxygen vacancies at the operating temperature of the sensors during the synthesis process. A typical metal oxide gas sensor can be described as an interactive material which interacts with the environment and generates a

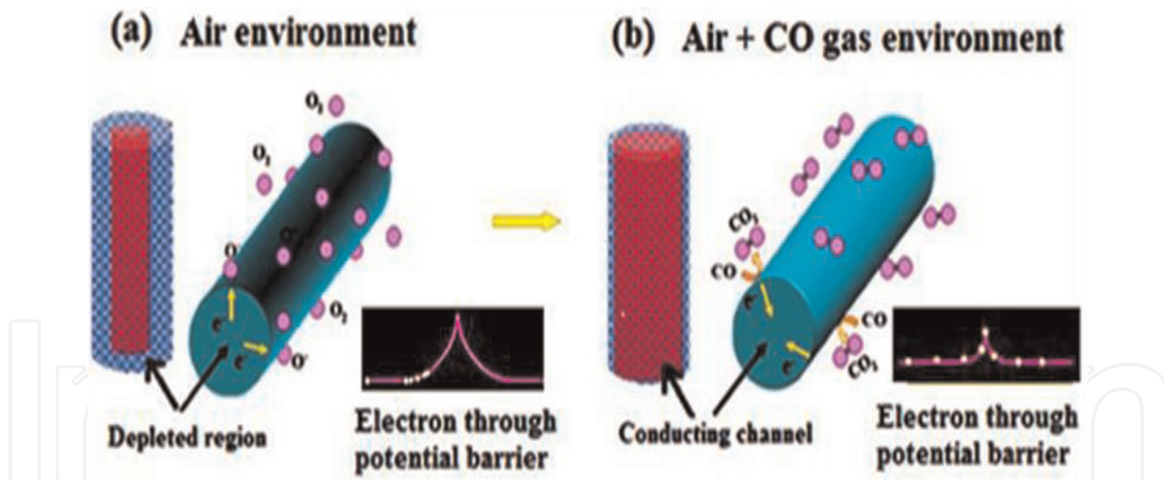


Figure 2. Schematic illustration of toxic chemical sensing process. (a) Adsorption of oxygen at surface of nanowires in air and creation of potential barrier and depletion region. (b) Modulation of potential barrier and depletion region after reaction of carbon monoxide (CO) at surface of n-type semiconductor.

response (as receptor) plus a device which reads the response and converts it into an interpretable and quantifiable term (as transducer).

2.4.1 Sensing mechanism of metal oxide semiconductor gas sensors

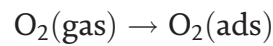
It is necessary to understand the sensing mechanism of the chemiresistive gas sensors for the subsequent chapters in this thesis. Since sensing mechanism of metal oxide semiconductor is mainly based on band theory, band theory can be applied to the gas sensor to explain the sensing mechanism. On interaction of the analytes (undetected) with the surface of nanostructures, these analytes react with attached oxygen ions on the surface of nanostructures; a change in the carrier concentrations of the material occurs. Due to the change in carrier concentrations of the material, the electrical resistivity of the materials changes. Decrease in resistivity (increase in conductivity) occurs for n-type metal oxide semiconductor on interaction of reducing gas [25]. So the sensing mechanism of oxide semiconductor is mainly based on the principle of modification in electrical properties (resistivity/conductivity) as a consequence of chemical reaction between gas molecules and the reactive oxygen ions on the surface of MOS nanostructure material. The sensing mechanism can be divided into three sections: (a) adsorption of oxygen at surface, (b) detection of gases by a reaction with adsorbed oxygen, and (c) change in resistance due to charge transfer at the surface.

2.4.2 Adsorption of oxygen at surface

Interactions of oxygen with the surface of a metal oxide semiconductor are of utmost importance in gas sensing mechanism. Oxygen is a strong electron acceptor on the surface of a metal oxide. Since the majority of sensors operate in an air at ambient temperature, therefore the concentration of oxygen on the surface is directly related to the sensor electrical properties. The conversion to O_2^- or O^- at prominent temperatures is useful in gas sensing mechanism, as only a monolayer of oxygen ions are present with these strongly chemisorbed species [26, 27]. Different forms of oxygen ions may be ionosorbed on the surface of metal oxide semiconductor nanostructures [28]. At low temperature ranges (150–200°C), molecules in the form of neutral O_2 or charged O^- are adsorbed. At higher temperature ranges above 200°C, atomic form of oxygen as O^- ions is adsorbed [29]. It is observed that

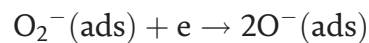
the reaction kinetics increase with increase in temperature. Sensors based on resistivity/conductivity properties (resistive sensors) work better at temperature of 300°C or above to react with ionosorbed oxygen at the surface. At temperature $T < 200^\circ\text{C}$, the following reactions take place at the surface of sensor (for physisorption):

$$E < (0.4 \text{ eV}) \quad (1)$$



At temperature $T > 200\text{--}400^\circ\text{C}$, the following reaction takes place at the surface of sensor (for chemisorptions):

$$E > (0.4 \text{ eV}) \quad (3)$$



Adsorption energy of oxygen on metals lies in the range of 4–6 eV. Extracted carriers originate from donor sites of the metal oxide surface in the material [30]. Intrinsic oxygen vacancies and other impurity defects give rise to donor sites and surface-trapped electrons. As a result of this, ionosorbed oxygen produces a depletion layer on the surface. A buildup charge is created on the surface of metal oxide semiconductors due to different events of adsorption, and this leads to upward band bending for n-type semiconductors [31].

2.5 Classification of nanomaterials

Over decades, the capability of varying surface morphologies and the structure of MOS with near atomic scale have led to further idealization of semiconductor structures: quantum wells, wires, and dots. These variations at nanoscale of metal oxide semiconductors have led to different concentrations and densities of electronic states. On the bases of their fundamental dimensions (x, y, and z) in space, nanostructures can be classified into 0-D (zero-dimensional), 1-D (one-dimensional), 2-D (two-dimensional), and 3-D (three-dimensional). 0-D nanostructures are quantum dots or nanoparticles; 1-D nanostructures are nanorods, nanowires, nanobelts, and nanotubes; 2-D nanostructures refer to nanosheets, nanowalls, and nanoplates; and 3-D nanostructures refer to nanoflowers and other complex structures such as nanotetrapods [32–34]. Quantum effects dominate most of the properties of the nanomaterials. There is a great difference between density of states of the nanomaterials and those of the bulk materials. The density of states which describe the electronic states versus energy in the band diagram of the 0-D, 1-D, 2-D, and bulk materials are shown in **Figure 3**.

2.6 Synthesis of ZnO nanostructures

Different methods are used for synthesis of ZnO nanostructures.

2.6.1 Vapor transport synthesis

Vapor transport process is one of the most common and cost-effective method used to synthesize ZnO nanostructures. In this process, ZnO vapors are transported usually by Argon (Ar) gas. Zinc (Zn) and oxygen (O) vapors can be generated by

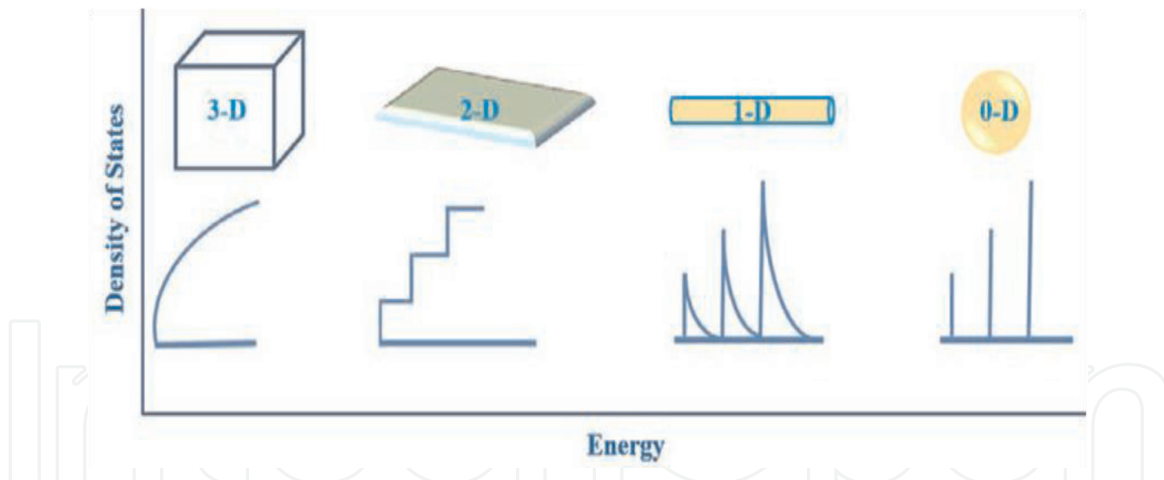


Figure 3.
The electron density of states in bulk metal oxide semiconductor and in that of quantum well (2-D), in quantum wire (1-D), and in quantum dot (0-D) nanomaterials.

different ways. Decomposition of ZnO is a direct and simple method; however due to high melting point of ZnO, it requires high temperature ($\sim 1975^{\circ}\text{C}$) [35]. To reduce the melting point of ZnO, graphite (C) powder is mixed with the same ratio with ZnO as a source material. At about $800\text{--}1000^{\circ}\text{C}$ temperature, graphite reduces the melting point of ZnO to form Zn and CO/CO₂ vapors. Zn and CO/CO₂ later react and result in ZnO nanostructures. The advantage of this method is that the existence of graphite significantly reduces the decomposition temperature of ZnO, i.e., graphite acts as a catalyst. On the bases of difference on nanostructure formation mechanisms, the vapor transport process can be divided into the following:

- i. Catalyst-free vapor-solid (VS) mechanism
- ii. Catalyst-assisted vapor-liquid-solid (VLS) mechanism

A rich variety of nanostructures, such as nanorods, nanowires, nanobelts, and other complex structures, can be synthesized by utilizing vapor-solid mechanism. In this mechanism, the nanostructures are produced by condensing directly from vapor phase. This mechanism is not so capable to provide best control on the geometry, alignment, and precise location of ZnO nanostructures.

Vapor-liquid-solid mechanism is a catalyst-assisted mechanism which is used for controlled growth of oxide semiconductor nanostructures. So nanowires, nanorods, and nanobelts have been achieved by VLS mechanism [36]. In this mechanism metals such as Au, Cu, Co, Sn, etc. are used as catalyst materials [37]. Alloy droplets are formed at high temperature as a result of the reaction between catalyst film and the substrate surface interface. In the growth of 1-D oxide nanostructures, the liquid droplet plays the role of nucleation sites for the precursor's vapors [38]. The vapors of the precursor are transported through carrier gases (usually noble gases are used as carrier gas) toward the substrate placed in the furnace tube during the growth of oxide semiconductor. During this process some materials are evaporated. The selection of catalyst is mainly based on its high surface tension and its high accommodation coefficient. These properties directly link with the supersaturation of the droplet with the source material vapors. The high Gibbs free energy carried by the precursor's vapors enables it to diffuse into the alloy droplet in order to minimize its energy.

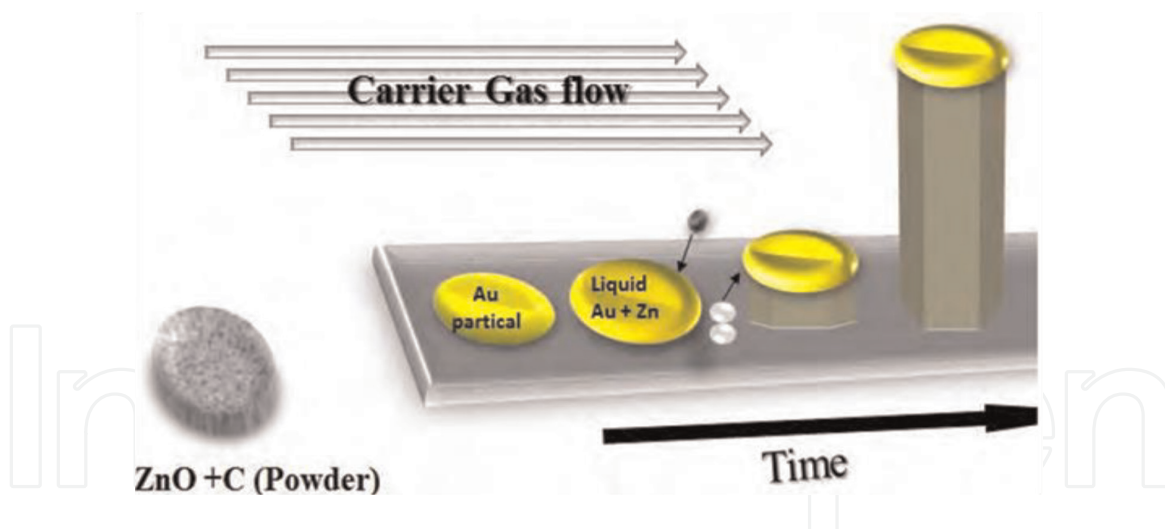


Figure 4. Schematic illustration of VLS mechanism for ZnO nanorod catalyst droplets at the tip of nanorods.

The supersaturation of liquid droplet (that acts as nucleation's site) with the source material vapors results in crystal structures of source material at the liquid-solid interface on the substrate, consequently forming one-dimensional nanostructure as shown in **Figure 4**.

2.6.2 Other synthesis methods

Despite the growth of 1-D oxide semiconductor nanostructures such as ZnO, GaN, and nanowires, the vapor transport process is the most dominant and cost-effective synthesis method; other growth methods such as electrochemical deposition (ECD), sol-gel, polymer assisted growth, etc. have been developed so far in parallel [39]. The possibility of forming ZnO nanostructures even at low temperature may be provided by these methods.

2.7 Catalyst effect on the growth of metal oxide semiconductors

Thickness of the catalyst layer coated on the substrate plays a vital role in the growth of MOS nanostructure materials by reducing the activation energy of the reaction without taking part in the chemical reaction.

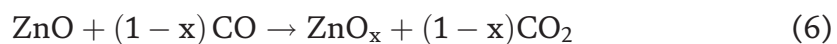
In supersaturation state catalyst droplet acts as a sink for source material in vapor-liquid-solid mechanism. The supersaturation level of droplet becomes smaller than the surrounding atmosphere's supersaturation level, when supersaturation of catalyst occurs. This difference creates a driving force, which drives the precursor vapors into the droplet, and growth of 1-D structures takes place in energetically favored crystallographic directions.

In vapor-solid mechanism, various types of substances are used as catalyst for the growth of 1-D nanostructures. The size and morphology of nanostructures can be controlled by using various types and thicknesses of catalysts. The finest catalyst has ideal rough surface whose sticking coefficient for the impinging of precursor material's atom from vapor phase is almost 1 [39].

2.8 Effect of gold catalyst on growth

Owing to its high surface tension, high accommodation coefficient, and high sticking power, gold (Au) is generally used as a catalyst in the synthesis of 1-D oxide nanostructure. Growth of 1-D oxide nanostructures with high crystallinity, density,

and long controlled diameter can be obtained by using Au as a catalyst. Growth of 1-D nanostructures has been reported by Borchers et al. with high density using Au catalyst [40]. ZnO nanowires can be grown through VLS mechanism by adding the catalyst substance which provides the nucleation sites for the growth of nanowires. The formation of these nuclei takes place through internal chemical reaction. This is considered to be a self-catalytic VLS growth. During the growth process, the reaction at low temperature can be fastening for vapor generation by adding some external materials in the source material. ZnO powder has a melting point of 1975°C, so pure ZnO does not sublime at 900–1100°C. So for this purpose carbon powder is mixed with ZnO powder with equal mass ratio that gives rise to the formation of Zn or Zn suboxide vapors at 1000°C [41], i.e.,



Various forms of ZnO nanostructures grow even at lower temperature because Zn or Zn suboxides act as nucleation sites for ZnO nanostructures. Other parameters like vacuum conditions, carrier gases, and catalysts are not essential in this condition. So the temperature is the only parameter that plays a vital role in the formation of various kinds of ZnO nanostructures. The formation of CO takes place by the direct reaction between graphite (C) and ZnO or O₂ depending upon the reaction condition (tube condition).

The formations of suboxides take place in open quartz tube due to the partially oxidized Zn vapor or droplet by the addition of graphite (C) at low melting temperature. Due to the high reactive power of suboxides as compared to ZnO, the deposition of zinc at the tips of grown nanostructures may increase during the synthesis process [42]. It is the main advantage of self-catalytic growth that impurity-free growth can be obtained as compared to catalyst-assisted growth of VLS.

2.9 Temperature effect on the growth of 1-D nanostructures

Temperature plays a crucial role in the growth of 1-D oxide nanostructures by thermal evaporation method through vapor-liquid-solid mechanism.

The thermodynamic phenomena like stability, dissociation adsorption, surface diffusion, and solubility of certain phases can be directly affected by temperature.

There are three types of ZnO fast growth direction from the structure point of view, namely, $\langle 2^{-1}^{-1}0 \rangle$, $\langle 01^{-1}0 \rangle$, and $\pm [0001]$, as shown in **Figure 5**. ZnO consists of various structures due to the polar surface activities of different growth facets. Every crystal has a unique crystal plane with different kinetic parameters, which are to be considered under controlled growth conditions.

The tetrahedral coordination of ZnO is shown, which has noncentral symmetry and piezoelectric effect [43, 44]. $[0001]$ is the fastest growing direction which is along the c-axis because its activation temperature is lower than other two directions. Due to activation, energy growth of nanorods with smaller lengths and diameters takes place at lower temperature, but when temperature increases, length and diameter of nanowires increase because the energy of this fast-growing direction $[0001]$ increases. At the higher temperatures, nanobelts with further increase in temperature facets $\langle 2^{-1}^{-1}0 \rangle$ and $\langle 0^{-1}^{-1}0 \rangle$ get high activation energies to grow nanosheets.

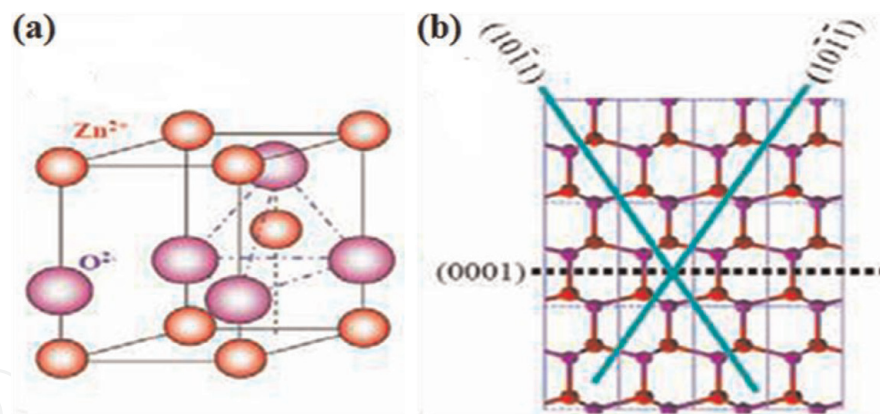


Figure 5.
(a) Wurtzite structure. (b) Growth direction model of ZnO.

2.10 Doping of nanostructures

Doping of the nanowires and nanorods through in situ or post processing techniques will provide a far more favorable approach to modulate their electrical, optical, and piezoelectric properties. Most metal dopant ions result in the increase of density of the conduction carriers by occupying the lattice sites in the ZnO crystal. The complete picture of the crystal can be changed by changing the doping level. The controlled modification of morphological features as well as enhancement of electrical and optical properties can be achieved by introducing dopant element in metal oxide semiconductor [45]. The electrical as well as optical properties of MOS can be tuned by adding the foreign elements or by the alternation of oxygen stoichiometry. By making these changes, one can get an increase in carrier's concentration, electrical resistivity, and mobility [45]. Doped nanostructure-based sensors are fully capable of sensing different harmful gases, with good stability, selectivity, and sensitivity. Out of many other methods, doping is considered to be one of the best methods for enhancement of gas sensing properties of ZnO nanostructures at room temperature. Doped ZnO nanostructures were used in the past by many researchers for the detection of harmful gases in the environment. For example, the gas sensing properties of Sn-doped ZnO nanostructures were investigated by S.C. Navel and I.S. Mulla using the thermal evaporation method. The results show good response to different gases for pure Sn-doped nanostructures, in temperature range of 275°C to 300°C. They proved that the sensitivity toward UV sensing can be increased by the doping of Sn material [46].

3. Experimental procedure

Experimental process comprises the following steps:

1. Preparation of substrate for growth
2. Coating of Au catalyst in ultrahigh vacuum (UHV) chamber on Si substrate
3. Preparation of nanostructure samples by vapor transport method through VLS mechanism
4. Fabrication of sensor for toxic gas sensing applications

3.1 Preparation of substrate for growth

By using the diamond cutter, Si substrates were cut in suitable sizes and shapes. In order to avoid the contamination, the substrates were cleaned before the deposition of catalyst, as oily layer and dust particles may stick to the surface of the substrates. For the cleaning purpose, the acetone was poured into a beaker, and the beaker was filled up to half level. The substrates were put into the acetone-filled beaker to completely immerse in them. The acetone-filled beaker was placed in ultrasonic bath at room temperature for 30 min. Si (100) substrates were then put into ethanol and deionized water for decontamination purpose for 30 min.

3.2 Deposition of Au catalyst on Si substrate in UHV chamber

For the growth of 1-D ZnO nanostructures, n-type silicon substrates Si (100) were used through the following steps:

1. Si substrates were cleaned in isopropyl alcohol (IPA), acetone, and deionized water (DI) by sonication to remove the contaminations in ultrasonic bath for 30 min at room temperature.
2. Sample substrates were loaded in the ultrahigh vacuum chamber for deposition of thin film of gold under vacuum of 10^{-7} Torr.
3. In nm, a thin layer of gold catalyst was deposited on Si (100) substrates for the growth of ZnO nanostructures.
4. Around 200 nm of thin layer of gold catalyst was deposited on Si (100) and glass substrates for preparation of sensor.
5. The samples were taken out from UHV chamber and used for growth process of ZnO nanostructures.

3.3 Preparation of samples by vapor transport method through VLS mechanism

The growth was performed by thermal evaporation in a temperature-controlled horizontal tube furnace by vapor transport process through VLS mechanism. An equimolar mixture (mixed in a ball mill for 2 h with 250 rpm) of ZnO (purity 99.99%) and graphite (purity 99.9%) was placed in a ceramic boat (88 mm of length) with a mass ratio 1:1 (measured by physical balance). This boat containing the source material (mixture of ZnO + C) was placed at the center of quartz tube (length 100 cm and diameter 3.5 cm). Tube furnace was set at a temperature of 850, 900, 950, and 1030°C for the four different experiments. Catalyst-coated substrates of 4 nm labeled as S1, S2, S3, and S4 were placed at the downstream of the source material at a distance of 18 cm (S1, 850°C), 12 cm (S2, 900°C), 9 cm (S3, 950°C), and 6 cm (S4, 1030°C), respectively. Furnace temperature was raised at the rate of 10°C per minute. At the start Ar gas (99.99%) was introduced at a rate of 50 standard cubic centimeter per minute (sccm) to flush out the residual present in the tube. Brass rod fitted in the rubber cork was inserted in the quartz tube to connect it to argon (Ar) gas source through a plastic pipe of 5 mm diameter. Argon gas was used as a carrier for transport of vapors from source material to gold-coated substrates. The other end of quartz tube was kept opened. The temperature of the furnace was increased from room temperature to 850°C (S1), 900°C (S2), 950°C

(S3), and 1030°C (S4) in four different experiments. When the temperature of the furnace reached the set temperature, the dwell or growth time was noted for 45 min. After 45 min the furnace program was “OFF,” and the temperature started decrease gradually. When the temperature decreased to 650°C, the Ar gas flow was switched “OFF.” Furnace was then cooled to room temperature after the reaction.

Doping of Mg was carried out, and for that purpose 0.05 g and 0.08 g of magnesium acetate $[\text{Mg}(\text{CH}_3\text{COO})_2 \cdot 4\text{H}_2\text{O}]$ (purity 99.99%) was added in 1 g of source material (ZnO + C). Mg-doped ZnO nanostructures were synthesized by thermal evaporation in a temperature-controlled horizontal furnace on an Au-coated Si (100) substrate. Vapor transport method has been used for the synthesis of Mg-doped ZnO nanostructures which was done in a temperature-controlled tube furnace. The temperature, growth time, and gas flow rate were 900°C, 45 min, and 50 sccm, respectively.

3.4 Sensor fabrication

The synthesized ZnO nanostructures were used for UV as well as for chemical sensing applications. ZnO nanostructures were annealed by heating it in digital

Samples	Source material	Catalyst used	Catalyst thickness (nm)	Synthesis temperature (°C)	Gas flow rate (sccm)	Growth time (min)
S1	ZnO + C	Au	4	850	50	45
S2				900		
S3				950		
S4				1030		

Table 1.
Sample details (synthesis temperature, gas flow rate, growth time).

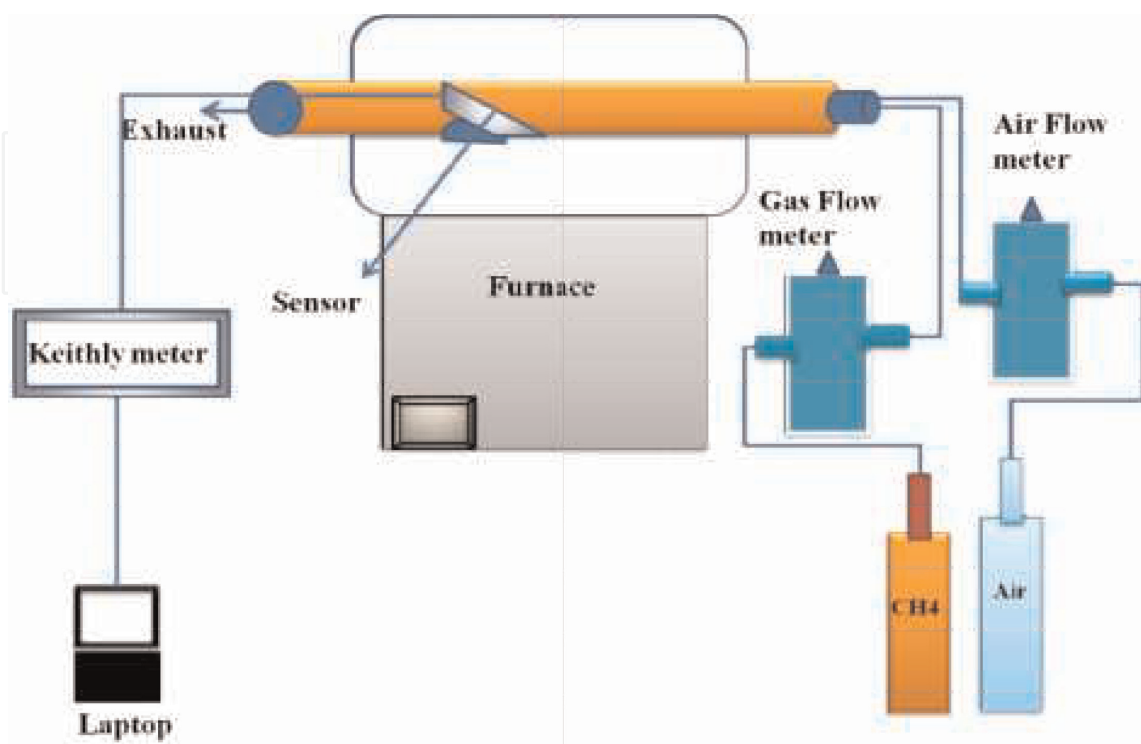


Figure 6.
Schematic illustration of chemical sensing experimental setup.

furnace at 400°C for 2 h. The annealing process was usually done for attachment of oxygen on the surface of ZnO nanostructures. The nanostructures were scratched with the help of blades, and the gaps or cuts on gold-coated quartz substrate were filled with the scratched nanostructures as shown in **Figure 6**. A small drop of methanol was dropped on the nanostructures with the help of 5 cc disposable syringe so that a thick paste was formed. The sensor was then placed under IR (infrared) light for 10 min for the purposes of sticking material on the quartz substrate. The experimental setup for chemical sensing is shown in **Figure 6**.

4. Morphological properties of ZnO nanostructures

Morphology, size, and shape of the synthesized ZnO nanostructures were characterized by using scanning electron microscopy (SEM) characterization technique. The four samples were synthesized at different temperatures with the same flow rate of 50 sccm of Ar (argon) gas and with same growth time of 45 min. A total eight samples was prepared in four different experiments; out of eight samples, four samples were optimized. Four experiments were done at different temperatures, i.e., 850, 900, 950, and 1030°C. The catalyst used was 4 nm thin layer of gold coated on n-type Si (100) substrate.

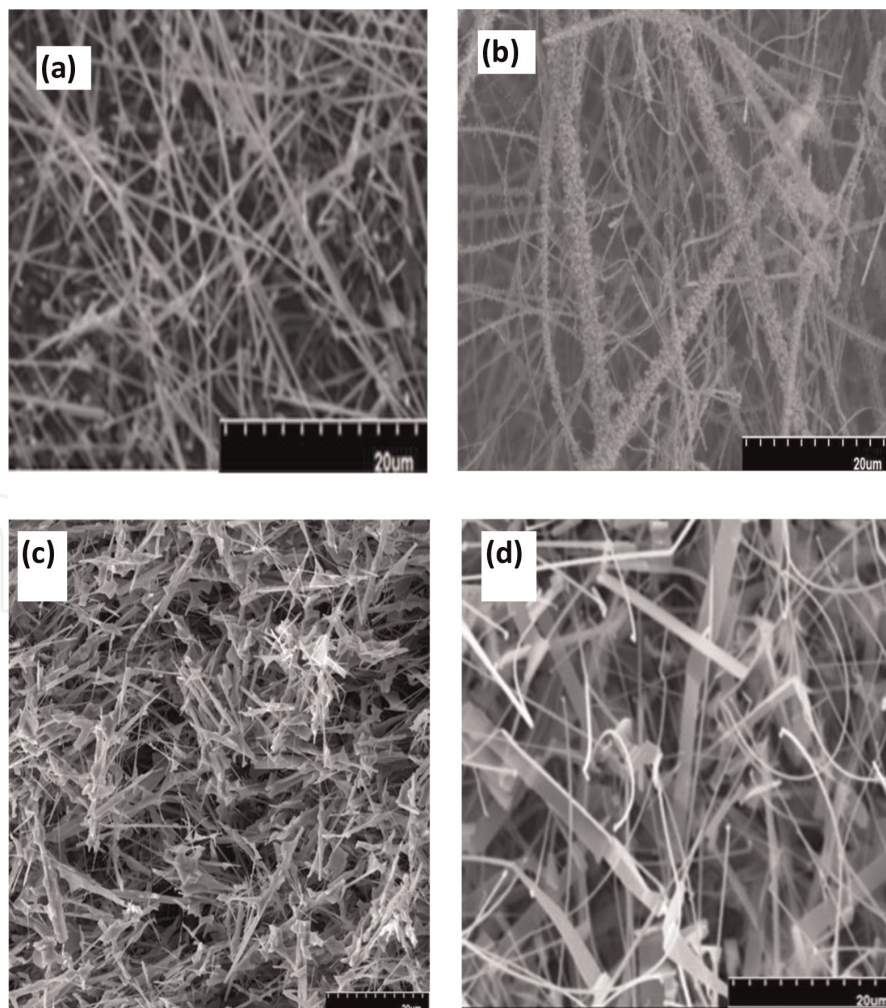


Figure 7. SEM images of different morphologies of ZnO nanostructures at different synthesized temperatures. (a) SEM images of nanowires grown at 850°C. (b) SEM images of nanorods grown at 900°C. (c) SEM images of nanobelts with needle-like ends grown at 950°C. (d) SEM images of nanobelts grown at 1030°C.

4.1 Sample S1

In the first experiment, ZnO nanowires with various dimensions were obtained. **Figure 7(a)** shows the SEM micrograph of the ZnO nanostructures of sample S1, consisting of randomly oriented ZnO nanowires. These nanowires were grown at a temperature of 850°C on a thin layer of pure gold-coated Si (100) substrate. The nanowires intertwine with each other and distribute on the whole substrate surface randomly. The average diameter and the average length are $0.95 \pm 0.11 \mu\text{m}$ and $35.59 \pm 9.90 \mu\text{m}$, respectively.

4.2 Sample S2

In the second experiment, ZnO nanorods of different dimensions were obtained. **Figure 7(b)** shows the SEM micrograph of complex ZnO nanorods of sample S2. These complex nanorods were grown at temperature of 900°C on a thin layer of gold-coated Si (100) substrate. The average diameter and the average length of S2 SEM images are $12.66 \pm 3.72 \mu\text{m}$ and $319.48 \pm 93.50 \mu\text{m}$, respectively.

4.3 Sample S3

In the third experiment, ZnO nanobelts with needle-like ends were obtained. **Figure 7(c)** shows the SEM micrograph of ZnO nanobelts of sample S3 with needle-like ends. These nanobelts were obtained with different dimensions at temperature of 950°C grown on 4 nm Au-coated thin layer of Si substrate. The average width, average length, and average thickness of tips are $1.39 \pm 0.44 \mu\text{m}$, $10.34 \pm 2.71 \mu\text{m}$, and $0.38 \pm 0.086 \mu\text{m}$, respectively.

4.4 Sample S4

Figure 7 shows the SEM micrograph of ZnO nanobelts of the fourth experiment which was grown at 1030°C on gold-coated Si substrate. The average length of $2.67 \pm 0.42 \mu\text{m}$, average width of $0.33 \pm 0.03 \mu\text{m}$, and the average thickness of $0.09 \pm 0.01 \mu\text{m}$ of nanobelts were obtained.

The scanning electron micrographs clearly showed that the morphologies tuned from nanowires and nanorods to nanobelts due to change in temperature. High temperature and supersaturation conditions lead to the formation of nanobelts with needle-like ends and typical nanobelts.

The possible reason for this tune in morphologies is attributed to supersaturation, growth rate, and quick availability of ZnO polar surfaces for growth [46]. Overall, the supersaturation conditions are different at different temperatures which eventually change the morphology.

4.5 Energy diffraction X-ray (EDX) analysis

EDX spectroscopy analytic technique was used for the chemical composition analysis of the synthesized ZnO nanostructures. **Figure 8** shows the typical EDX spectrum of the sample S1 (ZnO nanowires). Only the Zn, O, and Au peaks were observed. The observation of Au peak may suggest that the growth is catalyst-assisted [47–52]. The approximate atomic ratio was found to be 58:32. These ratios show nonstoichiometry, i.e., crystal defects of grown nanostructures during the growth process. Deviation from the stoichiometry is large due to carbothermal reaction and oxygen-deficient environment (Ar gas) during the growth process. Most of the oxygen is used in the formation of CO_2 , i.e.,

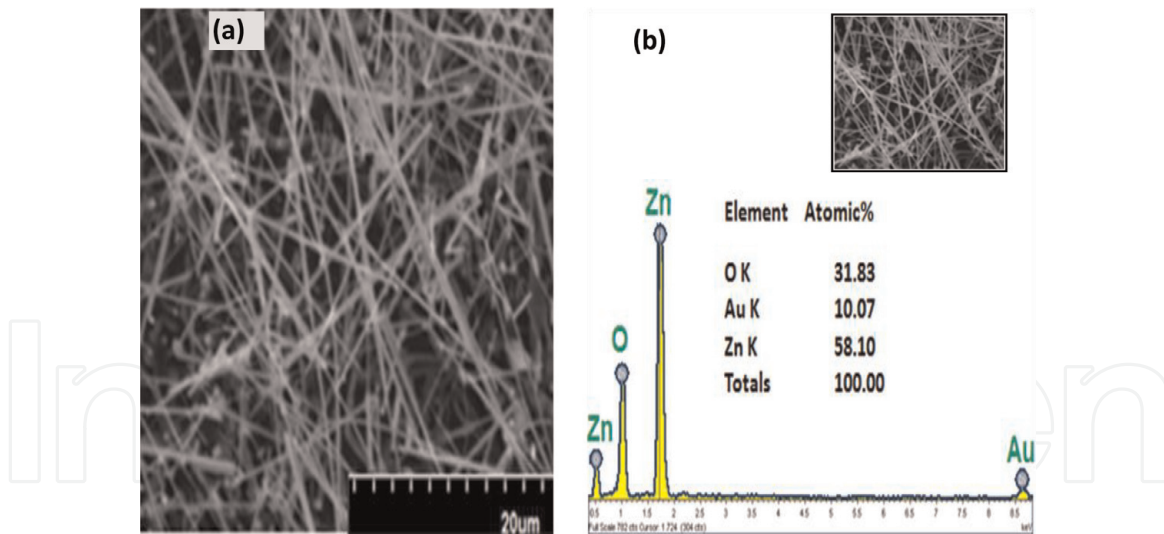


Figure 8.
 (a) SEM images of ZnO nanowires and (b) EDX image of the corresponding ZnO nanowires grown at 900°C.



4.6 Synthesis of Mg-doped ZnO nanostructures

The whole process of Mg-doped ZnO nanowires could be explained in two steps:

In the first step, a thin layer (4 nm) of Au film was coated on Si (100) substrate in UHV chamber by ion sputtering technique. Cleaning of Si (100) substrates was carried out by sonicating in acetone, ethanol, and deionized water for 30 min. Si (100) substrates were then coated with SiO₂ for 2 h at temperature of 1050°C for insulation purpose. The quartz tube was cleaned first with chromosulfuric acid (cleaning agent) to remove the permanent residue, then the deionized water was used to wash the tube, and last ethanol was used to clean the tube.

In the second step, the Mg-doped ZnO nanostructures were grown by vapor transport method through VLS mechanism in a temperature-controlled digital horizontal furnace as shown in the schematic illustration. In the first experiment, doping of sample S1 (nanowires) was carried out. A mixture of ZnO (purity 99.9%), magnesium acetate [Mg(CH₃COO)₂·4H₂O] (purity 99.99%), and graphite powders (carbon) with mass ratio in gram (weighted by physical balance) of 1:1:0.05 was used as the source materials. The source material was placed at the center of quartz tube of length 100 cm and diameter 3.5 cm in a ceramic boat of 88 mm length. Sample S1 substrate was placed on a second ceramic boat at the downstream at a distance of 18 cm away from the source materials in the quartz tube. The temperature of the furnace was maintained at 850°C.

At the start Ar gas was introduced at the rate of 50 sccm to flush out the residual present in the tube. As the temperature reached 850°C, the dwell time was noted for 45 min. After 45 min the furnace program was “OFF,” and the temperature started to decrease gradually. When the temperature decreased to 650°C, the Ar gas flow was switch “OFF.” Furnace was then cooled down to room temperature after the reaction. In the second experiment, Mg doping of sample S2 (ZnO nanorods) was carried out. The same condition and parameters were used for doping of S2, except

the magnesium acetate $[\text{Mg}(\text{CH}_3\text{COO})_2 \cdot 4\text{H}_2\text{O}]$ weight was 0.08 g, and the sample distance from the source material was 12 cm.

The collected Mg-doped ZnO nanostructure sample characterization was carried out for crystallinity, morphology and elemental composition, and optical properties. Optical and gas sensing response of the respective Mg-doped ZnO nanostructures was carried out by measuring respective resistances by two probe methods using a multimeter (Keithly 2100).

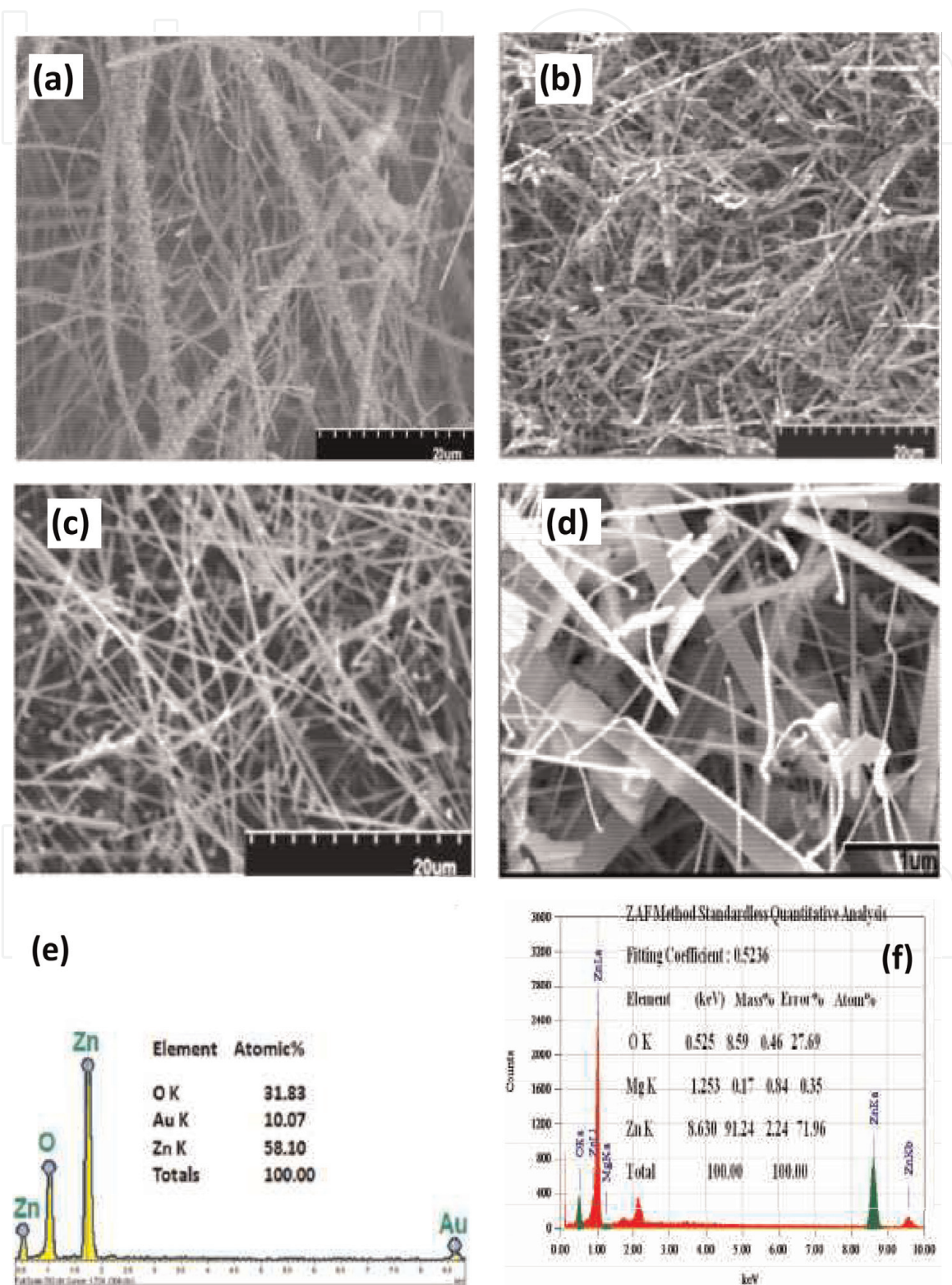


Figure 9. (a) SEM image of undoped ZnO nanorods (S2). (b) SEM images of Mg-doped ZnO nanobelts. (c) SEM image of undoped ZnO nanowires (S1). (d) SEM images of Mg-doped ZnO nanobelts. (e) and (f) show EDX analysis of undoped and Mg-doped ZnO nanowires and nanobelts, respectively.

4.7 Morphology analysis

Mg-doped ZnO nanostructure morphology was probed by means of SEM. **Figure 9(a)** shows the SEM image of undoped ZnO nanorods (S2) with average diameter and length of $12.66 \pm 3.72 \mu\text{m}$ and $319.48 \pm 93.50 \mu\text{m}$, respectively. **Figure 9(b)** shows SEM images of Mg-doped (0.05 g) ZnO nanobelts. The average thickness of $1.88 \pm 0.70 \mu\text{m}$, average width of $4.7 \pm 1.04 \mu\text{m}$, and average length of $72.03 \pm 18.84 \mu\text{m}$ of the Mg-doped ZnO nanobelts were measured. **Figure 9(c)** shows the SEM image of undoped typical ZnO nanowires (S1) with different dimensions, having average diameter and average length of $0.95 \pm 0.11 \mu\text{m}$ and $35.59 \pm 9.90 \mu\text{m}$, respectively. **Figure 9(d)** shows the respective EDX analysis spectrum of the undoped ZnO nanowires (S1). The EDX spectra show the attachment of O (oxygen) and Zn (zinc) in the ratio O/Zn which was found to be 32:58, respectively. These composition analyses clearly showed that no impurity peak was observed, showing the purity of ZnO nanostructures. The aspect ratio of undoped and doped ZnO nanorods and nanobelts was found to be 25 and 51, respectively. **Figure 9(e)** shows the Mg-doped (0.08 g) ZnO nanobelts having average thickness of $0.05 \pm 0.009 \mu\text{m}$, average width of $0.28 \pm 0.02 \mu\text{m}$, and average length of $2.93 \pm 0.87 \mu\text{m}$. The corresponding elemental compositions of the synthesized ZnO nanobelts were confirmed by EDX spectroscopy. **Figure 9(f)** shows the corresponding EDX analysis of the doped ZnO nanobelts, showing the presence of oxygen, magnesium, and zinc in the ratio O/Mg/Zn which was found to be 28:0.35:72 respectively. EDX analysis confirmed that the compositions of the products are Mg-doped ZnO without impurity. The aspect ratio of undoped ZnO nanowires and Mg-doped ZnO nanobelts was found to be 37 and 38, respectively. The possible reason for the formation of thin and transparent nanobelts is due to the morphology tuning from nanorods and nanowires to nanobelts by Mg doping, because doping of definite elements plays a key role in the alteration of the dimensions of nanostructures [52–58]. Growth rates and polar surfaces can provoke the asymmetric growth. Formation of nanobelts was explained as continuous process of 1-D branching and subsequent 2-D interspace filling.

Polar surfaces of wurtzite crystals of oxide semiconductors can induce asymmetric growth which leads to the diverse nanostructures, e.g., nanocombs, nanobrushes, needle-like belts/rods, etc. [59].

4.8 CH₄ gas sensing response

The first step was the preparation of CH₄ gas sensor. In the fabrication of CH₄ gas sensor, a thick layer (200 nm) of Au was coated by ion sputtering technique on Si (100) wafers. A small amount of ZnO nanostructures was put on a pair of interdigitated electrodes on Si substrates having a gap of 55 μm . A small drop of methanol was dropped on the nanomaterials so that a thick paste was formed. The annealing of sensors was carried out in an open furnace tube for 2 h at 400°C before performing the gas sensing experiments, for the purpose of attachment of oxygen on the surface of sensors. The sensing experiment was performed at 200°C with 5-min cycles of dry air and 400 ppm CH₄ gas concentration. The sensing response ($S = R_a/R_g$) of the device was measured by resistance change upon exposure to air (R_a) and CH₄ gas (R_g). **Figure 10(a)** and **(b)** shows the sensitivity response of CH₄ (methane gas) at 200°C for undoped ZnO nanowires and for Mg-doped ZnO nanobelts, respectively. Research papers showed that the sensitivity of the resistive sensors is highly affected by the Mg doping. The sensors were tested in a temperature range of 50–200°C for 400 ppm of CH₄ gas. Sensors show some response magnitude from 100°C temperature. Undoped ZnO nanowire sensors get its optimal point at 200°C

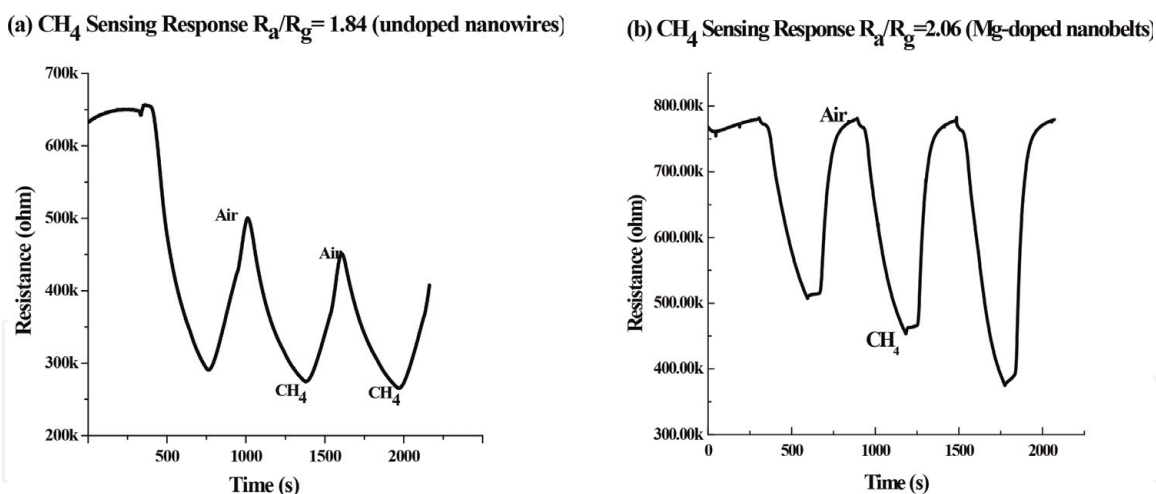


Figure 10.

(a) CH_4 gas sensing response of undoped ZnO nanowires (S_1). (b) CH_4 gas sensing response of Mg-doped ZnO nanobelts.

with response magnitude of 1.84. Doped ZnO nanobelts also get its optimal operating point at 200°C. Its response magnitude was obtained at 2.06. The best sensing signal response of CH₄ was found at 200°C. The sensing response at 50, 100, and 150°C (not shown) was comparatively negligible. The sensing response of undoped ZnO nanowires and Mg-doped ZnO nanobelts was found to be 1.84 and 2.06 at 200°C for the same concentration, respectively. The enhanced sensitivity response was observed for the ZnO nanostructures as shown in **Figure 10(b)**. Large amount of oxygen molecules and atoms are adsorbed on Mg-doped ZnO nanobelts due to large surface area (i.e., large defects are created) due to which interaction chance of CH₄ gas increases as compared to undoped ZnO nanostructures [60, 61]. On exposing the surface of the ZnO nanostructures to air, oxygen is adsorbed at the ZnO nanostructures surface by capturing an electron from conduction band of surface sites of undoped and Mg-doped ZnO nanostructures [62, 63]. Reactive O₂ (oxygen molecules) are chemisorbed or trapped by these ZnO nanostructures from the air, forming active oxygen species O₂⁻ and O⁻; as a result transformation of electrons takes place, due to which a wide space charge is formed that results in a decrease in carrier concentration due to which the resistance of the material is increased.

5. Conclusions

Growth of 1-D ZnO nanostructures was presented in the present chapter. Vapor-liquid-solid mechanism has been employed for the synthesis of ZnO nanostructures. It was found that the morphologies tuned with change in temperature which leads to the formation of nanowires at 850°C, nanorods at 900°C, nanobelts at 950°C, and nanobelts with needle-like ends at 1030°C. The dimensions of the morphologies have been measured by SEM. The length of the structures from 2.93 to 319.48 μm, thickness of the structures from 0.05 to 1.88 μm, and diameter of the structures from 0.95 to 12.66 μm have been obtained successfully. XRD peaks show that the crystallinity and intensity increase with increase in temperature. Doping of magnesium acetate (0.05 g) in ZnO through vapor transport method was successfully achieved. The sensing response of doped ZnO nanostructures for UV light at room temperature and CH₄ gas at 200°C has increased. ZnO nanowires show great selectivity response toward different volatile organic compounds (ethanol, methanol, and acetone). At the same concentration and temperature, the ZnO nanowires show

a huge sensing response to acetone (14), and those of the other solvents are no greater than 8.6.

Acknowledgements

The Higher Education Commission (HEC) of Pakistan is acknowledged for financial support through project No. 9294/NRPU/R&D/HEC/2017. Thanks to Prof. Dr. Syed Zafar Ilyas and Dr. Waqar. A. Syed. The authors would also be thankful to COMSATS University Islamabad for necessary funds for the project.

Conflict of interest

There is no conflict of interest in this chapter.

Author details

Nazar Abbas Shah^{1*}, Majeed Gul², Murrawat Abbas³ and Muhammad Amin²

¹ Thin Films Technology Laboratory, Department of Physics, COMSATS University, Islamabad, Pakistan

² Centre of Excellence in Science and Applied Technologies, Islamabad, Pakistan

³ NUST University, Islamabad, Pakistan

*Address all correspondence to: nabbasqureshi@yahoo.com

IntechOpen

© 2019 The Author(s). Licensee IntechOpen. This chapter is distributed under the terms of the Creative Commons Attribution License (<http://creativecommons.org/licenses/by/3.0>), which permits unrestricted use, distribution, and reproduction in any medium, provided the original work is properly cited. 

References

- [1] Roco MC, Mirkin CA, Hersam MC. Nanotechnology research directions for societal needs in 2020: Summary of international study. *Journal of Nanoparticle Research*. 2011;**13**(3):897
- [2] Chen P-C, Shen G, Zhou C. Chemical sensors and electronic noses based on 1-D metal oxide nanostructures. *IEEE Transactions on Nanotechnology*. 2008; **7**(6):668
- [3] Xiong HM et al. Sonochemical synthesis of highly luminescent zinc oxide nanoparticles doped with magnesium (II). *Angewandte Chemie International Edition*. 2009;**48**(15):2727
- [4] Maity R et al. Synthesis and characterization of ZnO nano/microfibers thin films by catalyst free solution route. *Physica E: Low-dimensional Systems and Nanostructures*. 2005;**25**(4):605
- [5] Qi Q et al. Humidity sensing properties of KCl-doped ZnO nanofibers with super-rapid response and recovery. *Sensors and Actuators B: Chemical*. 2009;**137**(2):649
- [6] Ivanov P et al. Development of high sensitivity ethanol gas sensors based on Pt-doped SnO₂ surfaces. *Sensors and Actuators B: Chemical*. 2004;**99**(2):201
- [7] Vander Wal R et al. Metal-oxide nanostructure and gas-sensing performance. *Sensors and Actuators B: Chemical*. 2009;**138**(1):113
- [8] Röck F, Barsan N, Weimar U. Electronic nose: Current status and future trends. *Chemical Reviews*. 2008; **108**(2):705
- [9] Zhou X et al. Humidity detection by nanostructured ZnO: A wireless quartz crystal microbalance investigation. *Sensors and Actuators A: Physical*. 2007; **135**(1):209
- [10] Iwanaga H et al. Growth mechanism of ZnO ribbon crystals from ZnS. *Journal of Crystal Growth*. 1976;**35**(2):159
- [11] Huang J, Wan Q. Gas sensors based on semiconducting metal oxide one-dimensional nanostructures. *Sensors*. 2009;**9**(12):9903
- [12] Lei B et al. Tuning electronic properties of In₂O₃ nanowires by doping control. *Applied Physics A*. 2004;**79**(3): 439
- [13] Kolmakov A, Moskovits M. Chemical sensing and catalysis by one-dimensional metal-oxide nanostructures. *Annual Review of Materials Research*. 2004;**34**:151
- [14] Dulub O, Boatner LA, Diebold U. STM study of the geometric and electronic structure of ZnO (0001)-Zn, (0001)-O, (1010), and (1120) surfaces. *Surface Science*. 2002;**519**(3):201
- [15] Meyer B, Marx D. Publisher's Note: Density-functional study of the structure and stability of ZnO surfaces [*Phys. Rev. B* 67, 035403 (2003)]. *Physical Review B*. 2003;**67**(3):039902
- [16] Spencer MJ. Gas sensing applications of 1D-nanostructured zinc oxide: Insights from density functional theory calculations. *Progress in Materials Science*. 2012;**57**(3):437
- [17] Bylander E. Surface effects on the low-energy cathodoluminescence of zinc oxide. *Journal of Applied Physics*. 1978;**49**(3):1188
- [18] Kasai PH. Electron spin resonance studies of donors and acceptors in ZnO. *Physical Review*. 1963;**130**(3):989
- [19] Yang X et al. Effect of post-thermal annealing on properties of ZnO thin film grown on c-Al₂O₃ by metal-organic

- chemical vapor deposition. *Journal of Crystal Growth*. 2003;**252**(1):275
- [20] Hong H-K et al. Portable electronic nose system with gas sensor array and artificial neural network. *Sensors and Actuators B: Chemical*. 2000;**66**(1):49
- [21] Hsueh T-J et al. Laterally grown ZnO nanowire ethanol gas sensors. *Sensors and Actuators B: Chemical*. 2007;**126**(2):473
- [22] Fine GF et al. Metal oxide semiconductor gas sensors in environmental monitoring. *Sensors*. 2010;**10**(6):5469
- [23] Barsan N, Weimar U. Understanding the fundamental principles of metal oxide based gas sensors; the example of CO sensing with SnO₂ sensors in the presence of humidity. *Journal of Physics: Condensed Matter*. 2003;**15**(20):R813
- [24] Kim H, Sigmund W. Zinc oxide nanowires on carbon nanotubes. *Applied Physics Letters*. 2002;**81**(11):2085
- [25] Sahm T et al. Basics of oxygen and SnO₂ interaction; work function change and conductivity measurements. *Sensors and Actuators B: Chemical*. 2006;**118**(1):78
- [26] Franke ME, Koplin TJ, Simon U. Metal and metal oxide nanoparticles in chemiresistors: Does the nanoscale matter? *Small*. 2006;**2**(1):36
- [27] Yamazoe N, Shimano K. Roles of shape and size of component crystals in semiconductor gas sensors I. Response to oxygen. *Journal of the Electrochemical Society*. 2008;**155**(4):185
- [28] Moulson AJ, Herbert JM. *Electroceramics: Materials, Properties, Applications*. John Wiley & Sons; 2003
- [29] Suehiro J et al. Dielectrophoretic fabrication and characterization of a ZnO nanowire-based UV photosensor. *Nanotechnology*. 2006;**17**(10):2567
- [30] Kumar S et al. Mechanism of ultraviolet photoconductivity in zinc oxide nanoneedles. *Journal of Physics: Condensed Matter*. 2007;**19**(47):472202
- [31] Bera A, Basak D. Carrier relaxation through two-electron process during photoconduction in highly UV sensitive quasi-one-dimensional ZnO nanowires. *Applied Physics Letters*. 2008;**93**(5):053102
- [32] Kind H et al. Nanowire ultraviolet photodetectors and optical switches. *Advanced Materials*. 2002;**14**(2):158
- [33] Lupan O, Chow L, Chai G. A single ZnO tetrapod-based sensor. *Sensors and Actuators B: Chemical*. 2009;**141**(2):511
- [34] Liu M, Kitai A, Mascher P. Point defects and luminescence centres in zinc oxide and zinc oxide doped with manganese. *Journal of Luminescence*. 1992;**54**(1):35
- [35] Studenikin S, Golego N, Cocivera M. Fabrication of green and orange photoluminescent, undoped ZnO films using spray pyrolysis. *Journal of Applied Physics*. 1998;**84**(4):2287
- [36] Alivisatos AP. Perspectives on the physical chemistry of semiconductor nanocrystals. *The Journal of Physical Chemistry*. 1996;**100**(31):13226
- [37] Zhang Y et al. Synthesis, characterization, and applications of ZnO nanowires. *Journal of Nanomaterials*. 2012;**2012**:20
- [38] Zhao W et al. Self-assembly of ZnO nanosheets into nanoflowers at room temperature. *Materials Research Bulletin*. 2008;**43**(11):3171
- [39] Liu D et al. Surface functionalization of ZnO nanotetrapods with photoactive and electroactive

organic monolayers. *Langmuir*. 2008; **24**(9):5052

[40] Kong XY, Wang ZL. Spontaneous polarization-induced nanohelices, nanosprings, and nanorings of piezoelectric nanobelts. *Nano Letters*. 2003;**3**(12):1625

[41] Leung Y et al. Zinc oxide ribbon and comb structures: Synthesis and optical properties. *Chemical Physics Letters*. 2004;**394**(4):452

[42] Yang P et al. Controlled growth of ZnO nanowires and their optical properties. *Advanced Functional Materials*. 2002;**12**(5):323

[43] Chang P-C et al. ZnO nanowires synthesized by vapor trapping CVD method. *Chemistry of Materials*. 2004; **16**(24):5133

[44] Wagner R, Ellis W. Vapor-liquid-solid mechanism of single crystal growth. *Applied Physics Letters*. 1964;**4**(5):89

[45] Li Y, Cheng G, Zhang L. Fabrication of highly ordered ZnO nanowire arrays in anodic alumina membranes. *Journal of Materials Research*. 2000;**15**(11):2305

[46] Johansson J et al. Growth related aspects of epitaxial nanowires. *Nanotechnology*. 2006;**17**(11):S355

[47] Borchers C et al. Catalyst-nanostructure interaction and growth of ZnS nanobelts. *Nanotechnology*. 2006; **17**(4):1067

[48] Wang N, Cai Y, Zhang R. Growth of nanowires. *Materials Science and Engineering: R: Reports*. 2008;**60**(1):1

[49] Wang ZL. ZnO nanowire and nanobelt platform for nanotechnology. *Materials Science and Engineering: R: Reports*. 2009;**64**(3):33

[50] Yang R, Ding Y, Wang ZL. Deformation-free single-crystal

nanohelices of polar nanowires. *Nano Letters*. 2004;**4**(7):1309

[51] Nguyen P et al. Epitaxial directional growth of indium-doped tin oxide nanowire arrays. *Nano Letters*. 2003; **3**(7):925

[52] Qin Y, Yang R, Wang ZL. Growth of horizontal ZnO nanowire arrays on any substrate. *The Journal of Physical Chemistry C*. 2008;**112**(48):18734

[53] Gilliland G. Photoluminescence spectroscopy of crystalline semiconductors. *Materials Science and Engineering: R: Reports*. 1997;**18**(3):99

[54] Manzoor U, Kim DK. Size control of ZnO nanostructures formed in different temperature zones by varying Ar flow rate with tunable optical properties. *Physica E: Low-dimensional Systems and Nanostructures*. 2009;**41**(3):500

[55] Brewster MM et al. The growth and optical properties of ZnO nanowalls. *The Journal of Physical Chemistry Letters*. 2011;**2**(15):1940

[56] Kwak EL et al. Anaplastic lymphoma kinase inhibition in non-small-cell lung cancer. *New England Journal of Medicine*. 2010;**363**(18):1693

[57] van Dijken A et al. The kinetics of the radiative and nonradiative processes in nanocrystalline ZnO particles upon photoexcitation. *The Journal of Physical Chemistry B*. 2000;**104**(8):1715

[58] Kang HS et al. Investigation on visible emission control of ZnO thin film. *Physica Status Solidi*. 2004;**1**(10): 2550

[59] Ahn SE et al. Photoresponse of sol-gel-synthesized ZnO nanorods. *Applied Physics Letters*. 2004;**84**(24):5022

[60] Manzoor U, Kim DK. Synthesis and enhancement of ultraviolet emission by post-thermal treatment of unique zinc

oxide comb-shaped dendritic
nanostructures. *Scripta Materialia*.
2006;**54**(5):807

[61] Han N et al. Photoluminescence
investigation on the gas sensing
property of ZnO nanorods prepared by
plasma-enhanced CVD method. *Sensors
and Actuators B: Chemical*. 2010;**145**(1):
114

[62] Prades JD et al. The effects of
electron-hole separation on the
photoconductivity of individual metal
oxide nanowires. *Nanotechnology*.
2008;**19**(46):465501

[63] Fan HJ et al. Vapour-transport-
deposition growth of ZnO
nanostructures: Switch between c-axial
wires and a-axial belts by indium
doping. *Nanotechnology*. 2006;**17**(11):
S231

IntechOpen